View metadata, citation and similar papers at core.ac.uk
brought to you by CORE
provided by CorpusUL

Crown ether modified peptide interactions with model membranes‡

Pierre-Alexandre Paquet-Côté[a], Matthieu Fillion[b], Marie-Ève Provencher[a], François Otis[a], Justine Dionne[b], Sébastien Cardinal[a], Barbara Collignon[c], Jochen Bürck[d], Patrick Lagüe[c], Anne S. Ulrich[d], Michèle Auger[b], Normand Voyer[a]*

[a]*Département de chimie and PROTEO, Université Laval, Québec, Canada;* [b]*Département de chimie, PROTEO, CERMA and CQMF, Université Laval, Québec, Canada;* [c]*Département de biochimie, de microbiologie et de bio-informatique and PROTEO, Université Laval, Québec, Canada;* [d]*Institute of Biological Interfaces (IBG-2), Karlsruhe Institute of Technology (KIT), Karlsruhe, Germany*

CONTACT : Normand Voyer, normand.voyer@chm.ulaval.ca, Département de chimie, Université Laval, Québec, QC, Canada

As a footnote on the first page: ‡ This paper is dedicated to the memory of our dear colleague and friend, Dr. Michèle Auger, who recently passed away.

Crown ether modified peptide interactions with model membranes‡

A simple model of an uncharged antimicrobial peptide, carrying four crown ether side chains, is modified further by the selective incorporation of arginine side chains to control its secondary structure and its interaction with model membranes and living cells. Conformational studies show that shifting the position of a cationic residue in the peptide sequence allows to control its secondary structure and supramolecular self-assembly in solution. Results also demonstrate that the secondary structure influences the interaction with model membranes and cells. An α-helical peptide with greater amphiphilicity forms assemblies that interact with both prokaryotic and eukaryotic model membranes and cells. However, a β-stranded peptide with evenly distributed charges generates assemblies that interact more selectively with prokaryotic model membranes and cells. In addition, we observed differences in peptide orientation between uncharged and cationic α-helical peptides with different phospholipid bilayers. In general, the studied peptides have a higher affinity for thinner membranes, and cationic peptides interacted better with anionic membranes.

Keyword: membrane active peptides, crown ethers, antimicrobial peptides, oriented circular dichroism, supramolecular assembly

Introduction

Interfacially active peptides have been widely studied over the past years. The many potential applications for these compounds show the diversity and the relevance of this research topic. Most of artificial ion channels (1,2), drug carriers and delivery cell-penetrating peptides (3,4), branched amphiphilic peptide capsules (5,6), antimicrobial peptides (7,8), and cytolytic peptides (8,9) are interfacially active peptides. Such superstructures have been widely studied for their interaction with lipid bilayer membranes.

However, despite all the new findings in this field, it remains challenging to engineer peptides with the desired properties using a rational design process. New active peptides are generally found by the discovery of new naturally occurring peptides (10,11), the specific modification of known peptides (11,12), or the high-throughput screening of a combinatorial library (13). As yet, there are few examples of studies using a rational peptide design method to achieve the desired effect and selectivity (14).

To better understand the molecular determinants that govern the interactions between interfacially active peptides and lipid membranes, our group has developed a 14-residue model peptide (**1**, Figure 1). It is made of a molecular backbone of ten leucines and four 21-crown-7 modified phenylalanines incorporated at positions 2, 6, 9 and 13. This model peptide was designed so that under an α-helix conformation, the crown ether side chains align on the same side of the helix to form an amphiphilic structure (15). Previous studies have shown that **1** induces membrane perturbation in a similar way antimicrobial and cytolytic peptides do (16). Indeed, **1** can induce the leakage of large fluorescent dyes encapsulated in phospholipid vesicles by forming supramolecular architectures (16). Its simple structure, its neutral charge (global net charge of 0) and its membrane perturbing activity make **1** an interesting model to study the effects of many parameters on the interaction between interfacially active peptides and lipid membranes.

We have previously studied membrane interactions of various analogues of **1** with different biophysical methods. Analogues of model peptide **1** bearing one cationic charge at all possible positions were studied for their interaction with model membranes (17,18). These analogues have a leucine substituted by a lysine, arginine or histidine at all possible positions. These studies reveal that the position of these charges has a profound influence on the secondary structure of the peptides and on their interaction with model membranes.

When a single positive charge is at position 3, 5, 10 or 12 in the sequence, the analogues keep the α-helical structure of **1** and induce high calcein leakage of zwitterionic and anionic vesicles. When the charge is at position 4, 7, 8 or 11, the analogues preferentially adopt a β-sheet secondary structure and induce high calcein leakage of anionic vesicles only, implying different supramolecular architectures with selective interfacial activity (17).

These differences in activity indicate a difference in their assemblies and in their modes of interaction with the lipid membranes, as shown by Lorin et al. (17,18). In a recent study (19), using solid-state NMR spectroscopy, polarized ATR-FTIR and dye-release fluorescent assays, our group investigated two analogues of **1,** known as R4R11 and R5R10 (Fig. 1), which respectively substitute leucines at positions 4 and 11, and at positions 5 and 10 for arginines. The choice to focus on these analogues was made because (i) arginine analogues of **1** are more active with model membranes and biological cells than other cationic amino acids and (ii) substitution of leucines by two cationic amino acids instead of one also improves the haemolytic activity profile and the antimicrobial activity (unpublished work). This study shows by various biophysical methods that these analogues interact with model membranes by a sinking-raft like mechanism with transient disordered toroidal pores. It also points to the importance of the amphiphilicity of these peptides on their insertion and interaction with model membranes.

The main purpose of this study is to shed light on the membrane interactions of interfacially active analogues R4R11 and R5R10 and their mono-arginine counterparts R4, R11, R5 and R10, using different biophysical, biological and computational methods.

Materials and methods

Synthesis.

The protected artificial amino acid (21-crown-7) L-phenylalanine was synthesised in solution from L-dopa and hexaethylene glycol, using a procedure we previously described (20,21). Model peptide **1** and its analogues, shown in Figure 1, were synthesised by solid phase peptide synthesis with N-Fmoc-protected amino acids and Wang resin using standard protocols (22-24). HOBt, HBTU, and DIPEA were used as coupling reagents, and 20% piperidine/DMF was used as deprotection conditions. After each coupling, a qualitative ninhydrin test was performed to verify the reaction completion. We obtained the desired analogues by cleaving the molecule with TFA/TIS.

All analogues were characterised by high performance liquid chromatography (HPLC) and high-resolution mass spectrometry (HRMS). Peptides with less than 95% crude purity were purified to homogeneity by semi-preparative HPLC. Additional details on the synthesis and on the characterisation of analogues are available in the supplemental material (SM).

Isotropic circular dichroism.

Studies were performed using small unilamellar vesicles (SUVs) of 1-palmitoyl-2-oleoyl-*sn*-glycero-3-phosphatidylcholine (POPC) or 1-palmitoyl-2-oleoyl-*sn*-glycero-3-phosphatidylglycerol (POPG) to mimic eukaryotic and prokaryotic cells, respectively. Dried lipids were hydrated with a 10 mM phosphate buffer solution at pH 7.0. First, multilamellar vesicles (MLVs) were formed by 5 cycles of vortexing, freezing (in liquid nitrogen) and thawing (in a water bath at 37°C). A final cycle of vortexing, freezing, and

thawing at room temperature was performed. Vesicles were extruded by passing the liposomal suspension 21 times through a polycarbonate membrane (0.1 μm diameter pores) using a mini-extruder (Avanti Polar Lipids). Then, the resulting suspension of large unilamellar vesicles (LUVs) was sonicated for 30 min. Finally, the obtained SUVs suspension was mixed with a crown ether peptide analogue to obtain a molar peptide/lipid (P/L) ratio of 1:60 and a final lipid concentration of 1 mg/mL. Spectra were acquired on a Jasco-815 spectropolarimeter with a 1 mm quartz glass cell at 37°C. The secondary structure composition was estimated for each spectrum using CDPro. Specific details on the spectral parameters, data acquisition, and processing are available in the SM.

Infrared spectroscopy.

IR studies were performed with peptide samples in the presence of large multilamellar vesicles (LMVs). First, peptides dissolved in 10 mM HCl were lyophilised at least five times. Samples were prepared by mixing a POPC or POPG solution in $CHCl_3$ with the appropriate amount of a peptide solution in $CHCl_3$/MeOH 1:1 to obtain a P/L ratio of 1:60. Mixtures were dried under a stream of nitrogen and dried under vacuum overnight to remove all traces of organic solvent. The dried samples were hydrated with a D_2O buffer solution (100 mM HEPES and 5 mM EDTA, pH 7.4) to obtain a final lipid concentration of 25% and hydration level of 80%. Five vortex/freeze/thaw cycles were performed to complete the preparation of LMVs. Samples were then deposited on CaF_2 windows and inserted in a thermoelectrically regulated homemade cell. Spectra were recorded at 37°C on a Nicolet Magna 560 spectrometer equipped with a nitrogen-cooled mercury-cadmium-telluride (MCT) detector. Specific details on the procedure and the data acquisition and processing are available in the SM.

Vesicle permeabilisation.

The assay (25) was performed to measure calcein leakage from large unilamellar vesicles (LUVs) of egg yolk phosphatidylcholine (EYPC) and egg yolk phosphatidylglycerol (EYPG). Vesicles were prepared by vortex mixing the dried lipids with an internal buffer (100 mM HEPES, 5 mM EDTA and 80 mM calcein at pH 7.4). The resulting mixtures were sonicated for 45 min and then filtered on a 0.2 μm cellulose acetate membrane. Vesicles were separated from free calcein by size-exclusion chromatography on a Sephadex-G50 column using an external buffer (100 mM HEPES, 5 mM EDTA and 200 mM NaCl at pH 7.4) as eluent. The final vesicle solution concentrations were determined with a Bartlett assay (26). Calcein leakage assays were performed by 500 seconds of monitoring the fluorescence increase triggered by the addition of an interfacially active peptide to the vesicle solution. Based on previous studies (17), we used a P/L ratio of 1:60. After 400 seconds of kinetic monitoring, 10 μL of a 10% Triton X-100 solution were added to assess the 100% of fluorescence. Fluorescence readings were recorded with a Varian Eclipse spectrofluorimeter using the Cary Eclipse Kinetics Application v1.1(133).

Haemolytic activity.

The peptides' haemolytic activity was determined using an assay adapted from Ryge (27) and Anantharaman (28). The assay was performed with ovine (sheep) red blood cells (RBC) that were collected from EDTA-treated blood by centrifugation at 2,000 x g for 15 min and stored in Alsever's solution at 4°C. Before the tests, RBCs were washed 3 times with phosphate-buffered saline (PBS: 10 mM phosphate buffer, 137 mM NaCl at pH 7.4), centrifuged at 1,000 x g for 5 min and then diluted with PBS to obtain a concentration of 10^8 cells/mL. For each assay, a 96-well plate was used. In each well 20 μL of the

erythrocyte solution was added to 170 µL of a PBS solution (50 mM phosphate buffer, 150 mM NaCl at pH 7.4) and 10 µL of a peptide solution in DMSO. Peptide solutions were prepared to give a final concentration of 100 µM. Plates were incubated at 37°C for 1 h and then centrifuged at 1,000 x g for 5 min to separate the undamaged erythrocytes. Then, 50 µL of the supernatant were transferred to a new plate and the haemoglobin concentration was measured from the absorbance at 414 nm. To calculate the haemolysis percentage for each plate, 0% haemolysis was determined from wells with 10 µL of pure DMSO and 100% haemolysis was measured from wells with 10 µL of DMSO with 2 µL of 10% Triton X-100 added to the solution.

Oriented circular dichroism.

The SUV suspensions were prepared with the desired peptide by premixing a lipid and a peptide solution in $CHCl_3$/MeOH 1:1 to obtain P/L ratios of 1:20, 1:50, 1:100, 1:200 and 1:500 and a total lipid quantity of 50 µg, 200 µg and 500 µg according to the experiment. After complete drying of the mixture, samples were hydrated with a 10 mM phosphate buffer (PB) solution at pH 7.0. Vesicles were then formed by ten vortex/freeze/thaw cycles and a 16 min sonication in a strong ultrasonic bath. Subsequently, vesicle suspensions were deposited on quartz glass plates as spots with 6 mm radius. The lipid amounts on the plate depending on the desired P/L ratio were kept between 50 and 500 µg. After drying, samples were hydrated overnight in a chamber in a 97% relative humidity atmosphere (K_2SO_4 saturated solution) above the phase transition temperature (at 30°C for 1,2-dimyristoyl-*sn*-glycero-3-phosphocholine (DMPC) and at room temperature for the others). For DMPC samples, measurements were achieved on a Jasco-810 spectropolarimeter in a custom-built cell (29) at 30°C and 97% relative humidity. For other lipid samples (i.e.: POPC,

POPC/POPG 1:1, 1,2-didecanoyl-*sn*-glycero-3-phosphatidylcholine (DDPC), 1,2-dilauroyl-*sn*-glycero-3-phosphatidylcholine (DLPC), 1,2-dimyristoleoyl-*sn*-glycero-3-phosphatidylcholine (DMoPC)), measurements were achieved on the UVCD-12 beamline at the KARA (former ANKA) synchrotron facility at KIT (30) using a custom-built cell at 23°C and 97% relative humidity. Additional details on the specific procedure and data acquisition and processing are available in the SM.

Molecular dynamics simulations

21-crown-7-modified phenylalanine parametrisation. A 21-crown-7-modified phenylalanine residue was built using PyMOL (The PyMOL Molecular Graphics System, Version 1.8 Schrödinger, LLC). The side chain parameters were assigned using the CHARMM General Force Field program version 2.2.0 (31-33) for the residue truncated at the benzene moiety. There was only one penalty of 40.2 for the dihedral angle parameter of the O-C-C-O atom combination that connects the crown ether to the benzene moiety. All other parameters had no penalty. The geometry of the truncated residue was optimised using CHARMM 41b1 (34) with 500 steps of Steepest Descent followed by 500 steps of Newton-Raphson, and the internal coordinates of the final conformation were used for the 21-crown-7-modified phenylalanine residue topology.

System preparation. Model peptide **1** and its positively charged analogues were built from internal coordinates in their elongated conformation using CHARMM. As the pKa of the termini are modulated by the environment of the membrane (35), two systems were built for each peptide: one with the default (charged) N- and C-termini, and another with neutral N- and C-termini. The peptides were oriented in the *xy* plan and translated 32

Å along the *z* axis. Then, 14 different configurations for each peptide were generated from random rotations around the origin along the *x*, *y* and *z* axis.

Implicit solvent simulations. Molecular dynamics (MD) simulations were carried out with CHARMM, using the CHARMM36m force field (36). The Generalised Born with a smoothed switching function (GBSW) implicit solvent method (37,38) combined with the replica exchange molecular dynamics (REXMD) simulations (39) was used to sample the peptide conformations at the membrane interface. With this approach, the lipid and the water molecules are not represented explicitly. Instead, with the GBSW implicit solvent method, the membrane is approximated as a solvent-inaccessible infinite planar low dielectric slab with a switching region at the dielectric boundary with the aqueous implicit solvent. A Generalised Born method is used for the electrostatic part and the solvent-exposed surface area for the nonpolar part with a phenomenological surface tension coefficient. The thickness of the implicit region was 28.5 Å and the switching length 1.5 Å each side of the implicit bilayer, corresponding approximately to the dimensions of a POPC bilayer (40). Non-polar interactions were taken into account using a surface tension coefficient of 0.005 kcal/(mol $Å^2$). For each peptide, and for both protonation states of the termini, 16 replicas with random orientations were produced, with temperatures ranging exponentially from 300 K to 600 K, using the MMTSB toolset (41). 40 ns trajectories were performed for each peptide for both protonation states of the termini, using a 2 fs timestep, with exchange of temperature between the replicas every 2 ps following the metropolis criterion. Cutoffs for the non-bonded interactions were 20 Å with a smoothing via a switching function over the range of 16.5 Å to 20 Å.

Trajectory analysis. Peptide conformations at 300 K were extracted from the last 4 ns of trajectories. Secondary structures were evaluated using the DCLIKE method of wordom 0.22 - rc3 (42). The typical conformation was the conformation with the lowest RMSD from the average structure, evaluated using wordom.

Results and discussion

Isotropic circular dichroism.

The conformation of the analogues was investigated in presence of POPC and POPG vesicles, using circular dichroism (CD) to evaluate the effect of the charged residue's position on the secondary structure (Figure 2). Qualitative analysis of the R5, R10 and R5R10 spectra shows patterns similar to a typical α-helix structure with both POPC and POPG vesicles. This is marked by a maximum around 192 nm and two minima around 208 nm and 222 nm. This indicates that the structure for these peptides is mainly an α-helix. These observations are confirmed by the estimation of the secondary structure performed on these spectra (Table 1). It shows that the main conformation is the α-helix, ranging from 48 to 87%.

Figure 2 also reveals that for analogues R4, R11 and R4R11, spectra show a higher proportion of β-sheet structures with a maximum around 196 nm and one minimum around 216 nm. For R4 and R11, this corroborate with the secondary structure estimation (Table 1) showing between 39 and 48% of β-sheet with both type of lipids. However, the estimation of R4R11 shows 44% of α-helix and 24% of β-sheet for POPC and 51% of α-helix and 22% of β-sheet for POPG. A proportion of α-helix higher than expected according to the

CD spectra (Figure 2). This can be explained by the low reliability of the common algorithms to evaluate peptides and proteins adopting unusual β-structures or rich in β-sheets(43,44).

In addition, control experiments on all analogues of peptide **1** were performed in a phosphate buffer solution without phospholipids (Figure S1). The solubility of these peptides without vesicles is low. This ensue that secondary structures estimation cannot be done reliably. However, qualitative analysis of the spectra shows patterns similar to an α-helix structure for R5 and R5R10 and to a β-sheet structure for R4R11. For R4, R10 and R11, the signal is too weak to interpret their spectra.

These results agree with data obtained previously (17) with lysine-substituted crown ether peptide analogues: lysine substituted peptides K4, K11 and K4K11 (equivalent to R4, R11, R4R11) fold mainly in a β-sheet conformation in the presence of phospholipid vesicles, whereas K5, K10 and K5K10 adopt mainly an α-helix conformation. This emphasises the fact that the secondary structure of these peptides in solution is influenced mainly by the position of the cationic charge residue in the sequence and their interaction with crown ether side chains.

Infrared spectroscopy.

The results obtained by CD coincide with those obtained with infrared spectroscopy studies. Information about the secondary structure are observed in the 1700 to 1550 cm^{-1} region. This region features the C=O stretching vibration band of the amide group known as the amide I' band. This band is well known to be sensitive to the secondary structure of peptides and proteins. Spectra (Figure 3) show well-defined and narrow amide I' absorption bands characterised by a small full width at half height (FWHH) (data available in the SM

Table S1).

These well-defined bands allow us to identify the presence of secondary structure in the analogues. Peptides R4 and R11 with POPC vesicles (Figure 3A) have their main amide I' absorption band at 1623 cm^{-1} and a second smaller band at 1681 cm^{-1} corresponding to what is expected for an intermolecular β-sheet secondary structure (45,46). A third and smaller band is observed at 1652 cm^{-1} that can be attributed to a weak contribution of an α-helical structure. The spectra of R4 and R11 with POPG vesicles (Figure 3B) have the same characteristics as with POPC. The main noticeable difference is the narrower band suggesting a better homogeneity of the secondary structures, indicating a higher proportion of intermolecular β-sheets. Spectra of R5 and R10 with POPC (Figure 3A) show a main absorption band at 1652 cm^{-1} corresponding to an α-helical structure. Even if the band appears to be a little broader than the main bands of R4 and R11, it has a small FWHH and is quite symmetric, which indicates that the α-helix structure is predominant for these peptides. The only other spectral feature noticeably present is a small shoulder around 1620 cm^{-1}, which corresponds to a slight contribution of intermolecular β-sheets to the solution structure of R5 and R10. The spectra measured in POPG (Figure 3B) show again a narrowing of the main band compared to the POPC spectra, indicating a higher proportion of α-helices. This can be attributed to the interaction with the anionic vesicles that promotes the stability of the α-helical secondary structures for these analogues.

R4R11 and R5R10 analogues have spectra similar to their mono-arginine counterparts. R4R11 with POPC (Figure 3C) shows the characteristic band of intermolecular β-sheet with a slightly higher contribution of other secondary structure compared to the R4 and R11. This is seen by the smaller relative intensity of the main band at 1621 cm^{-1} compared to the region between 1640 and 1680 cm^{-1}. Again, with POPG

(Figure 3D), the spectra are similar but narrower than with POPC (Figure 3C). It is plausible to say that interfacially active peptide R4R11 interacts more strongly with POPG membranes, which lead to a more defined β-sheet structure. Finally, R5R10 upon interacting with POPC (Figure 3C) or with POPG (Figure 3D) shows that it mainly adopts an α-helical structure, as seen by a narrow band at 1652 cm^{-1}. These results confirmed those previously obtained by ATR-FTIR with DMPC and DMPG LMVs showing that R4R11 adopts an intermolecular β-sheet structure and R5R10 adopts an α-helical structure (19). In addition, there are two bands centred at 1610 and 1585 cm^{-1} for all analogues. These bands correspond to the antisymmetric and symmetric N-H stretching of the guanidine moiety of the arginine residues respectively (45,47).

The IR results support those obtained by circular dichroism. Indeed, analogues R5, R10 and R5R10 preferentially adopt an α-helical conformation in the presence of POPC or POPG vesicles, whereas analogues R4, R11 and R4R11 preferentially adopt a β-sheet conformation in the presence of POPC or POPG vesicles. Overall, the IR results confirm that there are no substantial conformational differences for all crown ether peptide analogues studied when they interact with POPC or POPG vesicles.

The preferred secondary structures of these analogues can be explained by the complexation of the crown ether moieties with the cationic guanidinium group of the arginine residue. When there is an arginine at positions 5 or 10, an α-helical conformation favours the closest spatial proximity of the cationic residue and the crown ether, therefore stabilising the helix. When the cationic amino acid is at positions 4 or 11, it is the β-sheet conformation that allows the closest spatial proximity of the two binding moieties, hence making β-sheets the most stable conformation.

Vesicle permeabilisation.

The vesicle permeabilisation assay gives information on the global peptide interaction with model lipid membranes. Results are reported in Table 2. With zwitterionic model membranes (EYPC), results show that model peptide **1** has a high calcein leakage, indicating a strong interaction with the model membrane, which causes vesicle permeabilisation. Addition of an arginine to the structure can cause an increase or decrease in calcein leakage, depending on the position of the amino acid. Incorporation of an arginine at position 4 or 11 causes a large decrease in the interaction with the zwitterionic model membrane, as seen for R4 and R11. However, if the amino acid is at position 5 or 10, the interaction is increased. When two arginines are introduced to the crown ether peptide, the interaction is decreased regardless of the position, as shown with R4R11 and R5R10. Still, if the arginines are at positions 4 and 11, this decrease goes near 0% of calcein leakage (3%), in comparison to positions 5 and 10, which still generate 32% of leakage. These results show that the interactions with zwitterionic model membrane (EYPC) decreases with the number of arginines, with the more significant decreases are observed with R4, R11 and R4R11.

This is consistent with previous calcein leakage assay studies using DMPC vesicles that showed the same trends with analogues of **1** with one arginine, histidine or lysine residue at these same positions (17). A trend is observed when we compare these results with the secondary structure of the analogues. The ones adopting mostly a β-sheet structure are those with a decreased interaction with EYPC vesicles, whereas the ones that prefer an α-helical conformation induce higher calcein leakages.

Calcein leakage results with EYPG vesicles show the same trends. R4, R11 and R4R11 are the less active peptides. R5, R10 and R5R10 generally induce a higher leakage compared to R4, R11 and R4R11. Again, these results agree with the previous studies with DMPG vesicles (17) with similar analogues bearing one histidine, lysine or arginine. It is noteworthy that in comparing the interactions of R4R11 with EYPC and with EYPG, we observed that in the first case there is almost no permeabilisation (3%) and in the second vesicles permeabilisation increases to 24%. This shows a preference for the R4R11 peptide for anionic membranes, in agreement with our previous results (17) with the analogue having two lysine residues at positions 4 and 11. This selectivity is most likely caused by the β-sheet conformation that R4R11 adopts in the presence of phospholipid vesicles, since this is the main difference between R5R10 and R4R11. In addition, the difference in conformation influences the amphiphilicity of the peptides. Indeed, R5R10 has a greater amphiphilic character, with its cationic charges on the same side of the helix as the crown ethers. Contrarily, R4R11 has a reduced amphiphilic character, as the charges are more distributed along the β-structure. Amphiphilicity has been shown to be a major factor in the membrane leakage activity of interfacial active peptides (48). These results confirm those previously obtained (19) with POPC and POPG vesicles showing that R5R10 have similar permeabilisation activity with the two types of vesicles and that R4R10 have a higher permeabilisation activity with POPG vesicles.

Haemolytic activity.

The interaction of the interfacially active peptides with a natural membrane was assessed by a haemolytic assay using ovine RBC. The results obtained (Table 2) show that model peptide **1** has no haemolytic activity at 100 μM. The incorporation of a cationic charge at

position 4 or 11, or even at both positions, does not increase haemolysis, as shown by absence of activity of analogues R4, R11 and R4R11. However, incorporation of arginines at positions 5 or 10 results in significant increases of haemolytic activity. Indeed, R5 almost completely lyses RBC (98%), whereas R10 induced lysis in 44% of the RBC used in the assay. Interestingly, using crown ether peptide R5R10 led to the same level of haemolysis as R10, showing that a cationic charge at position 10 mitigates the haemolytic activity related to the cationic charge at position 5. These results underscore the impact of the positive charge's position on the haemolytic activity, as compared to the global net charge of the interfacially active peptides. For the same net charge of +1, R4, R5, R10 and R11 have significantly different activities where only the position of a cationic charge is changed. This is also observed for R4R11 and R5R10 with a net charge of +2, with no and 45% haemolytic activity, respectively.

These results are consistent with those obtained with an EYPC model membrane. Peptides with mainly β-sheet secondary structure with arginines at positions 4 and/or 11 do not cause permeabilisation of model zwitterionic membrane or natural eukaryotic membrane. Peptides with mainly α-helical structure with arginines at positions 5 and/or 10 permeabilise model zwitterionic membranes and natural eukaryotic membranes. Again, these results show that the amphiphilicity of the α-helical peptides plays a major role in the haemolytic activity with interfacially active peptides.

Orientational studies.

Oriented CD spectroscopy is a powerful technique to study the interactions of helical peptides with bilayer membranes. The orientation of α-helical peptides in lipid bilayers can be observed by measuring a CD spectrum when a bilayer sample is oriented perpendicular

to the light beam (49,50). If the peptide lies parallel to the surface of the bilayer (i.e. the helix axis perpendicular to the beam, S-state), the spectrum is similar to a typical α-helix spectrum, with a maximum at 192 nm and two minima around 208 and 222 nm, where the corresponding "fingerprint" CD band around 208 nm will exhibit maximum negative amplitude. However, if the peptide is inserted perpendicularly within the bilayer (i.e. the helix axis parallel to the beam, I-state), the minimum at 208 nm undergoes a decrease in negative ellipticity and it approaches zero or even positive values due to the overlapping positive band around 192 nm. Since this technique only applies for α-helical peptides, R4, R11 and R4R11 could not be studied.

First, the exact position of the short-wavelength minimum was determined by acquisition of spectra in vesicle suspension (isotropic conditions). These spectra showed the fingerprint band position at 210 nm for **1** and at 208 nm for R5R10 with POPC vesicles and it shifts to 209 nm for **1** and to 207 nm for R5R10 with POPC/POPG 1:1 vesicles. Model peptide **1** was first studied at a different P/L ratio with POPC bilayers (Figure 4A). The spectra at P/L ratios of 1:100, 1:200 and 1:500 are characterised by a 210 nm band less intense than the 222 nm band, indicating that the crown ether peptide is partially inserted in the bilayer. When the P/L ratio was increased to 1:50 and then to 1:20, the negative ellipticity of the band was even closer to zero, signifying a greater insertion of peptide **1** into the lipid bilayer. However, since the band is not at zero or in the positive, **1** is not completely inserted in the membrane. This state can be called a tilted state (T-state) that can be described by a peptide unit obliquely inserted in the lipid bilayer with a stable slant. Although, this result can also be explained by having (i) two stable populations in both I- and S-state or (ii) by a rapid insertion equilibrium between peptides in I-state and S-state. These results suggest that **1** is in a T-state that tends toward an S-state at low concentration

and at higher concentrations it tends toward an I-state, where all peptide units would be inserted perpendicular to the bilayer. This phenomenon can be explained by a supramolecular effect due to the self-assembly of several model peptides **1** into supramolecular architectures that prefer the low-polarity environment of bilayer membranes.

To confirm whether the phospholipid head group influences the orientation of the peptide, studies were made at different P/L ratios with POPC/POPG 1:1 (Figure 4B). At the lowest concentration studied, P/L 1:200, model peptide **1** is almost exclusively in an S-state, oriented parallel to the lipid bilayer. This is shown by the more pronounced negative ellipticity of the band at 209 nm compared with the one at 222 nm. An increase in concentration of **1** induces a decrease in intensity of the band, suggesting a re-orientation of the peptide toward a T-state. However, the spectra with POPC/POPG 1:1 molar ratio have a higher relative intensity of the 209 nm band than the corresponding spectra obtained with pure POPC. This suggests stronger interactions between the neutral peptide **1** and the anionic head groups, potentially involving crown ether cation complexation, leading to a decrease in incorporation inside the bilayer.

The same studies were performed with the R5R10 analogue. The bis-arginine peptide spectra with the POPC bilayer at all P/L ratios (Figure 5A) show a strong negative band at 208 nm. This indicates that at all concentrations, the peptide prefers an S-state and stays in parallel alignment with respect to the surface of the bilayer. These results are in agreement with those previously obtained using solid-state NMR showing that R5R10 seems to have a mode of action similar to a sinking-raft mechanism with POPC membranes (19). This mode of action involves disordered toroidal pores (51) where the peptides do not align perpendicular to the membranes as in the conventional toroidal pores. With a

POPC/POPG 1:1 membrane, spectra (Figure 5B) are also characterised by a strong 207 nm band at low concentrations, indicating an S-state. However, increasing the concentration leads to a reduced amplitude of the 207 nm band. This is especially true at the highest P/L ratio of 1:20, indicating that interfacially active peptide R5R10 adopts a T-state at high P/L ratio in a POPC/POPG membrane. These results confirm that interactions between the cationic peptide R5R10 and an anionic lipid bilayer favours a more tilted orientation and increases the insertion of the peptides within the bilayer.

Model peptides **1** and R5R10 were further investigated for their incorporation into lipid bilayers of different thickness and at a P/L ratio of 1:100. Five different lipids with decreasing thickness were studied: POPC, DMPC, DMoPC, DLPC and DDPC. The isotropic spectra of the two peptides are similar in the presence of all types of phospholipids, with a minimum at 210 nm for **1** and at 208 nm for the R5R10 (data not shown).

Using POPC, the spectra obtained for **1** (Figure 6A) show that the peptide exists in a slightly tilted alignment, as previously observed. When the bilayer's membrane thickness decreases, ellipticities at the 210 nm band move toward positive values, indicating an increased incorporation of peptides into the thinner bilayers, and even reaching a complete I-state for model peptide **1** with the DMoPC, DLPC and DDPC bilayers. The spectra obtained for the R5R10 peptide (Figure 6B) show a similar tendency. The spectrum with POPC has a more pronounced minimum at 208 nm, which indicates a stronger S-state. When the bilayer thickness decreases, the ellipticities at this band move toward positive values, indicating an increased incorporation of peptides within the thinner bilayers. The two peptides are completely inserted in the two thinner bilayers of DLPC and DDPC.

This bilayer thickness effect can be explained by the mismatch between the helical peptide length and the bilayer thickness. With thicker bilayers like POPC, the peptide length is too short to completely span the hydrophobic core of the membrane when inserted. Therefore, the peptide prefers to remain mainly at the surface in an S-state or partially inserted in a T-state. However, when peptide **1** or R5R10 interact with thinner bilayers, like DLPC and DDPC, their hydrophobic length better match the hydrophobic thickness of the bilayer of these phospholipids. This condition facilitates membrane incorporation, thus favouring an I-state over an S-state. Our group previously observed (52) this behaviour with longer crown ether peptides acting as ion channels.

Overall, the orientational studies indicate that model peptide **1** is partially incorporated in zwitterionic phospholipid bilayers of POPC and is less incorporated in the presence of anionic phospholipids (POPG). Cationic peptide R5R10 prefers to sit on the surface of zwitterionic phospholipid bilayer (POPC) and is more incorporated in the presence of anionic phospholipids (POPG). In addition, because these peptides have lengths that match better the hydrophobic layer thickness, they are more incorporated in thinner bilayers.

Molecular dynamics simulations.

In order to shed light on the conformations and the membrane interactions of model peptide **1** and its analogues, we performed *in silico* MD simulations. Crown ether peptides were modelled using the GBSW implicit solvent model with the replica exchange sampling method using 16 replicas at different temperatures. Two systems were built for each peptide: one with the default (charged) N- and C-termini, and another with neutral N- and C-termini, for a total of 14 systems. Each replica was constructed in an elongated

conformation and positioned and oriented randomly relatively to the centre of the implicit membrane. Each system was subjected to 40 ns of replica exchange molecular dynamics simulations. The results were calculated using the conformations at the lowest temperature extracted from the last 4 ns of each trajectory.

Figure 7 presents the typical structures extracted from the last 4 ns of trajectory for the peptides with the charged termini (for the typical structures for the peptides with neutral termini, see SM Figures S9-S15). Overall, for peptides with both charged and neutral termini, the crown ether peptides take position at the interface of the implicit bilayer. Some peptides adopt a stable amphiphilic helical structure preferring to lay down at the surface of the bilayer (peptide **1**, R5, R10 and R5R10), while the other peptides have their secondary structure less ordered. In general, the crown ether moieties point toward the polar solvent and interact with a nearby positive residue (arginine or N-terminus). These last interactions determine the secondary structure adopted by the peptide. On the other side, the hydrophobic leucine chains generally insert into the hydrophobic interface of the implicit bilayer, serving as anchoring groups to the bilayer.

The percentages of the secondary structure elements are presented in Figure 8 for peptide **1** and the positively charged analogues. As observed from the isotropic circular dichroism and the infrared studies in the presence of lipid vesicles (Figures 2 and 3), Figure 8 shows that for analogues R4, R11 and R4R11 the helical content is the lowest, while the helical content is higher for peptide **1**, R5, R10 and R5R10, for both peptides with charged and neutral termini. The typical structures presented in Figures 7 and S9-S15 suggest that the helical content is prescribed by the interactions of the crown ethers with the arginines and the N-termini. Except for R4R11, the peptide helical conformation is stabilised in presence of a neutral N-terminus, as observed from the lower helical content for residues 3-

5 of the charged N-terminus peptides (see SM Figures S16-S22). In contrast, the arginines at positions 4 and 11 reduce the helical content of the R4, R11 and R4R11 analogues, while the arginines at positions 5 and 10 provide a helical content similar to values observed for peptide **1**.

The low β-sheet content of peptides R4, R11 and R4R11 observed from the simulations is in contrast with the experimental CD and IR results (Figures 2 and 3). This divergence suggests that the secondary structure of these peptides is stabilised from interactions with other molecules, such as another peptide or lipids. However, such intermolecular interactions could not be reproduced in our simulations, as we included only one peptide per system and we used an implicit membrane to computationally afford the peptide folding simulations. Therefore, we were not able to reproduce the atomic details of the peptide-peptide and peptide-lipid molecular interactions that might be necessary for proper peptide folding.

Overall, simulations demonstrate that a single unit of the crown ether modified 14 residues peptide prefers to sit flat on the surface of a bilayer membrane. Hence, well defined supramolecular architectures are necessary to favour incorporation into the hydrophobic core of a bilayer membrane. Such superstructures can only be formed upon increasing the concentration of the crown ether peptides.

Conclusion

We investigated the effects of the incorporation of cationic arginine charges into the structure of a simple crown-ether-modified peptide on its interfacial activity with lipid membranes. The results indicate that the position of the cationic charge is one of the main

molecular determinants that dictate the interaction and interfacial activity with membranes, whether the membrane is negatively charged or zwitterionic. The results also show that modification of only one amino acid can significantly alter the secondary structure of a 14-residue peptide and, therefore, its interfacial activity with different types of membranes. The phospholipid headgroups' charge and the membrane thickness also impact the interaction of all α-helical peptides and change their degree of incorporation into bilayers. Overall, the biophysical data and MD simulations reported for all crown ether peptides support a supramolecular mechanism necessary to form well-defined architectures with several peptide units to incorporate into the hydrophobic core of bilayer membranes in a stable I-state. More work is necessary to determine the detailed supramolecular structure of the multiple peptide architectures that can be stable in a bilayer membrane.

This study has permitted a better understanding of the molecular determinants involved in the membrane interfacial activity of amphiphilic peptides. Information gained will help in the rational design of new antimicrobial peptides with improved activity and selectivity.

Acknowledgements

This work was supported by the Natural Sciences and Engineering Research Council of Canada (NSERC), the Fonds de recherche du Québec-Nature et Technologies (FRQNT), and the Quebec Network for Research on Protein Function, Engineering, and Applications (PROTEO). P.-A.P.-C. acknowledges a graduate scholarship from FRQNT and from the CREATE Training Program in Bionanomachines (CTPB). P.-A. P.-C. also thanks the CTPB for an international fellowship. The authors thank Renée Bazin and Patrick Trépanier from Héma-Québec for their technical assistance with the haemolytic assay. We acknowledge the KIT light source for provision of instruments at the beamline UV-CD12 of the Institute of Biological Interfaces (IBG2) and we would like to thank the Institute for Beam Physics and Technology (IBPT) for the operation of the storage ring, the

Karlsruhe Research Accelerator (KARA) and Bianca Posselt and Siegmar Roth for their assistance with the SR-OCD measurements.

REFERENCES

(1) Bukovnik, U.; Gao, J.; Cook, G.A.; Shank, L.P.; Seabra, M.B.; Schultz, B.D.; Iwamoto, T.; Chen, J.; Tomich, J.M. *Biochim. Biophys. Acta, Biomembr.* **2012,** *1818,* 1039-1048.
(2) Chung, L.A.; Lear, J.D.; DeGrado, W.F. *Biochemistry* **1992,** *31,* 6608-6616.
(3) Marks, J.R.; Placone, J.; Hristova, K.; Wimley, W.C. *J. Am. Chem. Soc.* **2011,** *133,* 8995-9004.
(4) Guidotti, G.; Brambilla, L.; Rossi, D. *Trends Pharmacol. Sci.* **2017,** *38,* 406-424.
(5) Sukthankar, P.; Avila, L.A.; Whitaker, S.K.; Iwamoto, T.; Morgenstern, A.; Apostolidis, C.; Liu, K.; Hanzlik, R.P.; Dadachova, E.; Tomich, J.M. *Biochim. Biophys. Acta, Biomembr.* **2014,** *1838,* 2296-2305.
(6) Avila, L.A.; Chandrasekar, R.; Wilkinson, K.E.; Balthazor, J.; Heerman, M.; Bechard, J.; Brown, S.; Park, Y.; Dhar, S.; Reeck, G.R.et al. *J. Controlled Release* **2018,** *273,* 139-146.
(7) Ageitos, J.M.; Sanchez-Perez, A.; Calo-Mata, P.; Villa, T.G. *Biochem. Pharmacol.* **2017,** *133,* 117-138.
(8) Moreno, M.; Giralt, E. *Toxins* **2015,** *7,* 1126-1150.
(9) Zhao, H.; Qin, X.; Yang, D.; Jiang, Y.; Zheng, W.; Wang, D.; Tian, Y.; Liu, Q.; Xu, N.; Li, Z. *Cell Death Discovery* **2017,** *3,* 17037.
(10) Moe, M.K.; Haug, T.; Sydnes, M.O.; Sperstad, S.V.; Li, C.; Vaagsfjord, L.C.; de la Vega, E.; Stensvåg, K. *J. Nat. Prod.* **2018,** *81,* 140-150.
(11) Luna-Ramirez, K.; Tonk, M.; Rahnamaeian, M.; Vilcinskas, A. *Toxins* **2017,** *9,* 22.
(12) Porto, W.F.; Irazazabal, L.; Alves, E.S.F.; Ribeiro, S.M.; Matos, C.O.; Pires, Á.S.; Fensterseifer, I.C.M.; Miranda, V.J.; Haney, E.F.; Humblot, V.et al. *Nat. Commun.* **2018,** *9,* 1490.
(13) Rathinakumar, R.; Walkenhorst, W.F.; Wimley, W.C. *J. Am. Chem. Soc.* **2009,** *131,* 7609-7617.
(14) Tossi, A.; Sandri, L.; Giangaspero, A. *Biopolymers* **2000,** *55,* 4-30.
(15) Ouellet, M.; Otis, F.; Voyer, N.; Auger, M. *Biochim. Biophys. Acta* **2006,** *1758,* 1235-1244.
(16) Vandenburg, Y.R.; Smith, B.D.; Biron, E.; Voyer, N. *Chem. Commun.* **2002***,* 1694-1695.
(17) Lorin, A.; Noël, M.; Provencher, M.E.; Turcotte, V.; Masson, C.; Cardinal, S.; Lagüe, P.; Voyer, N.; Auger, M. *Biochemistry* **2011,** *50,* 9409-9420.
(18) Lorin, A.; Noël, M.; Provencher, M.E.; Turcotte, V.; Cardinal, S.; Lagüe, P.; Voyer, N.; Auger, M. *Biophys. J.* **2012,** *103,* 1470-1479.
(19) Fillion, M.; Goudreault, M.; Voyer, N.; Bechinger, B.; Auger, M. *Biochemistry* **2016,** *55,* 6919-6930.
(20) Biron, E.; Otis, F.; Meillon, J.C.; Robitaille, M.; Lamothe, J.; Van Hove, P.; Cormier, M.E.; Voyer, N. *Bioorg. Med. Chem.* **2004,** *12,* 1279-1290.
(21) Boutin, J.M.; Richer, J.; Tremblay, M.; Bissonette, V.; Voyer, N. *New J Chem* **2007,** *31,* 741-747.
(22) Wang, S.S. *J. Am. Chem. Soc.* **1973,** *95,* 1328-1333.
(23) Fields, G.B.; Noble, R.L. *Int. J. Pept. Protein Res.* **1990,** *35,* 161-214.
(24) Arseneault, M.; Dumont, M.; Otis, F.; Voyer, N. *Biophys. Chem.* **2012,** *162,* 6-13.
(25) Benachir, T.; Lafleur, M. *Biophys. J.* **1996,** *70,* 831-840.
(26) Bartlett, G.R. *J. Biol. Chem.* **1959,** *234,* 469-471.
(27) Ryge, T.S.; Doisy, X.; Ifrah, D.; Olsen, J.E.; Hansen, P.R. *J. Pept. Res.* **2004,** *64,* 171-185.
(28) Anantharaman, A.; Rizvi, M.S.; Sahal, D. *Antimicrob. Agents Chemother.* **2010,** *54,* 1693-1699.
(29) Bürck, J.; Roth, S.; Wadhwani, P.; Afonin, S.; Kanithasen, N.; Strandberg, E.; Ulrich, A.S. *Biophys. J.* **2008,** *95,* 3872-3881.

(30) Bürck, J.; Roth, S.; Windisch, D.; Wadhwani, P.; Moss, D.; Ulrich, A.S. *J. Synchrotron Radiat.* **2015,** *22,* 844-852.
(31) Vanommeslaeghe, K.; Raman, E.P.; MacKerell, A.D. *J. Chem. Inf. Model.* **2012,** *52,* 3155-3168.
(32) Vanommeslaeghe, K.; MacKerell, A.D. *J. Chem. Inf. Model.* **2012,** *52,* 3144-3154.
(33) CGenFF interface. https://cgenff.umaryland.edu (accessed Oct 14, 2018).
(34) Brooks, B.R.; Brooks, C.L.; Mackerell, A.D.; Nilsson, L.; Petrella, R.J.; Roux, B.; Won, Y.; Archontis, G.; Bartels, C.; Boresch, S.et al. *J. Comput. Chem.* **2009,** *30,* 1545-1614.
(35) Teixeira, V.H.; Vila-Viçosa, D.; Reis, P.B.P.S.; Machuqueiro, M. *J. Chem. Theory Comput.* **2016,** *12,* 930-934.
(36) Huang, J.; Rauscher, S.; Nawrocki, G.; Ran, T.; Feig, M.; de Groot, B.L.; Grubmüller, H.; MacKerell Jr, A.D. *Nat. Methods* **2016,** *14,* 71-73.
(37) Im, W.; Feig, M.; Brooks, C.L. *Biophys. J.* **2003,** *85,* 2900-2918.
(38) Im, W.P.; Lee, M.S.; Brooks, C.L. *J. Comput. Chem.* **2003,** *24,* 1691-1702.
(39) Sugita, Y.; Okamoto, Y. *Chem. Phys. Lett.* **1999,** *314,* 141-151.
(40) Kučerka, N.; Nieh, M.-P.; Katsaras, J. *Biochim. Biophys. Acta, Biomembr.* **2011,** *1808,* 2761-2771.
(41) Feig, M.; Karanicolas, J.; Brooks, C.L. *J. Mol. Graphics Modell.* **2004,** *22,* 377-395.
(42) Seeber, M.; Felline, A.; Raimondi, F.; Muff, S.; Friedman, R.; Rao, F.; Caflisch, A.; Fanelli, F. *J. Comput. Chem.* **2011,** *32,* 1183-1194.
(43) Khrapunov, S. *Anal. Biochem.* **2009,** *389,* 174-176.
(44) Micsonai, A.; Wien, F.; Kernya, L.; Lee, Y.-H.; Goto, Y.; Réfrégiers, M.; Kardos, J. *Proc. Natl. Acad. Sci. U. S. A.* **2015,** *112,* E3095-E3103.
(45) Barth, A. *Biochim. Biophys. Acta, Bioenerg.* **2007,** *1767,* 1073-1101.
(46) Surewicz, W.K.; Mantsch, H.H.; Chapman, D. *Biochemistry* **1993,** *32,* 389-394.
(47) Chirgadze, Y.N.; Fedorov, O.V.; Trushina, N.P. *Biopolymers* **1975,** *14,* 679-694.
(48) Matsuzaki, K. *Biochim. Biophys. Acta, Biomembr.* **2009,** *1788,* 1687-1692.
(49) Olah, G.A.; Huang, H.W. *J. Chem. Phys.* **1988,** *89,* 2531-2538.
(50) Wu, Y.; Huang, H.W.; Olah, G.A. *Biophys. J.* **1990,** *57,* 797-806.
(51) Sengupta, D.; Leontiadou, H.; Mark, A.E.; Marrink, S.-J. *Biochim. Biophys. Acta, Biomembr.* **2008,** *1778,* 2308-2317.
(52) Savoie, J.-D.; Otis, F.; Bürck, J.; Ulrich, A.S.; Voyer, N. *Pept. Sci.* **2015,** *104,* 427-433.

Table 1. Secondary structure estimation from the circular dichroism spectra.

Peptide	Lipid	Secondary structure proportion[a] (%)			
		α-helix	β-sheet	β-turn	Random coil
R4	POPC	2 ± 1	48 ± 2	22 ± 0	28 ± 1
	POPG	9 ± 1	39 ± 0	21 ± 0	31 ± 1
R5	POPC	71 ± 1	5 ± 1	8 ± 1	16 ± 1
	POPG	79 ± 2	3 ± 1	5 ± 1	13 ± 2
R10	POPC	51 ± 1	10 ± 1	13 ± 1	25 ± 1
	POPG	48 ± 2	13 ± 1	13 ± 1	26 ± 1
R11	POPC	3 ± 1	43 ± 2	23 ± 1	30 ± 1
	POPG	12 ± 3	43 ± 3	21 ± 1	25 ± 3
R4R11	POPC	44 ± 3	24 ± 3	17 ± 1	15 ± 2
	POPG	51 ± 5	22 ± 3	16 ± 2	12 ± 1
R5R10	POPC	60 ± 3	9 ± 2	8 ± 1	23 ± 2
	POPG	56 ± 2	9 ± 2	12 ± 1	24 ± 1

a) Estimated from the spectra in Figure 2 using CDPro. Additional information in SM

Table 2. Calcein leakage and haemolytic activity of **1** and its cationic analogues.

Peptide	Calcein leakage[a] (%)		Haemolysis (%)
	EYPC vesicles	EYPG vesicles	at 100 μM
1	60 ± 4	89 ± 8	1 ± 3
R4	17 ± 14	10 ± 2	-1 ± 0
R5	87 ± 0	87 ± 12	98 ± 13
R10	78 ± 3	34 ± 9	44 ± 9
R11	7 ± 5	11 ± 3	-1 ± 0
R4R11	3 ± 2	24 ± 6	-1 ± 1
R5R10	32 ± 5	34 ± 15	45 ± 11

a) Calcein leakage from LUVs of EYPC and EYPG at a peptide/lipid ratio of 1:60.

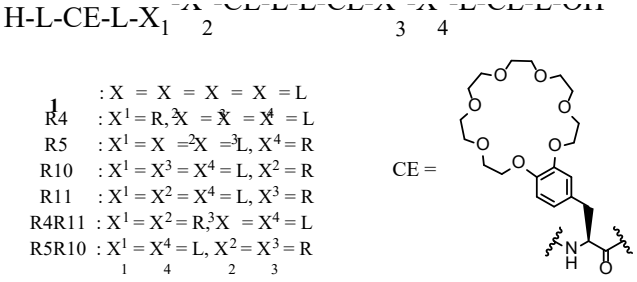

Figure 1. Sequence of model peptide **1** and its positively charged analogues used in this study.

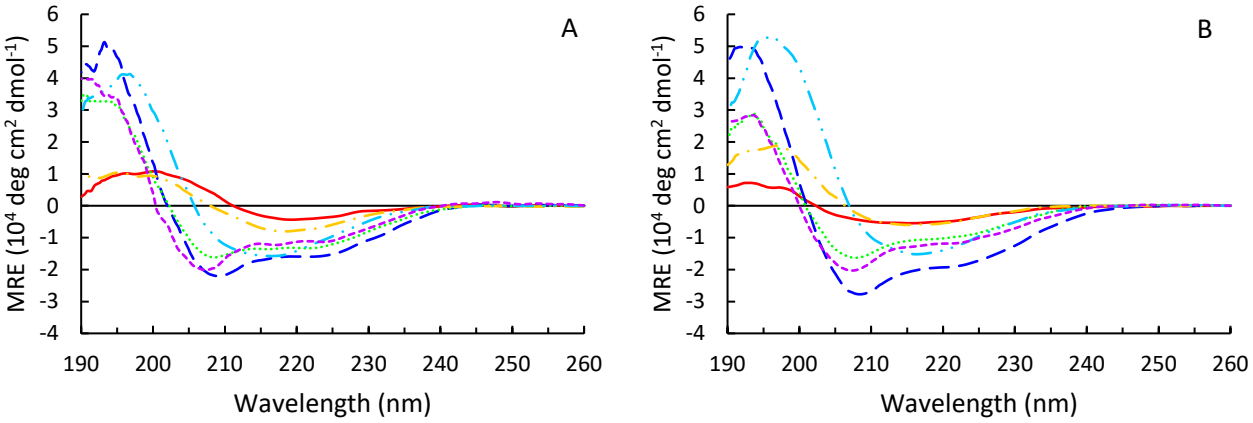

Figure 2. CD studies in mean residue ellipticity (MRE) of all analogues with (A) POPC and (B) POPG vesicles at P:L ratios of 1:60 at 37°C: R4 (—), R5 (– – –), R10 (· · ·), R11 (– · –), R4R11 (– · · –) and R5R10 (- - -).

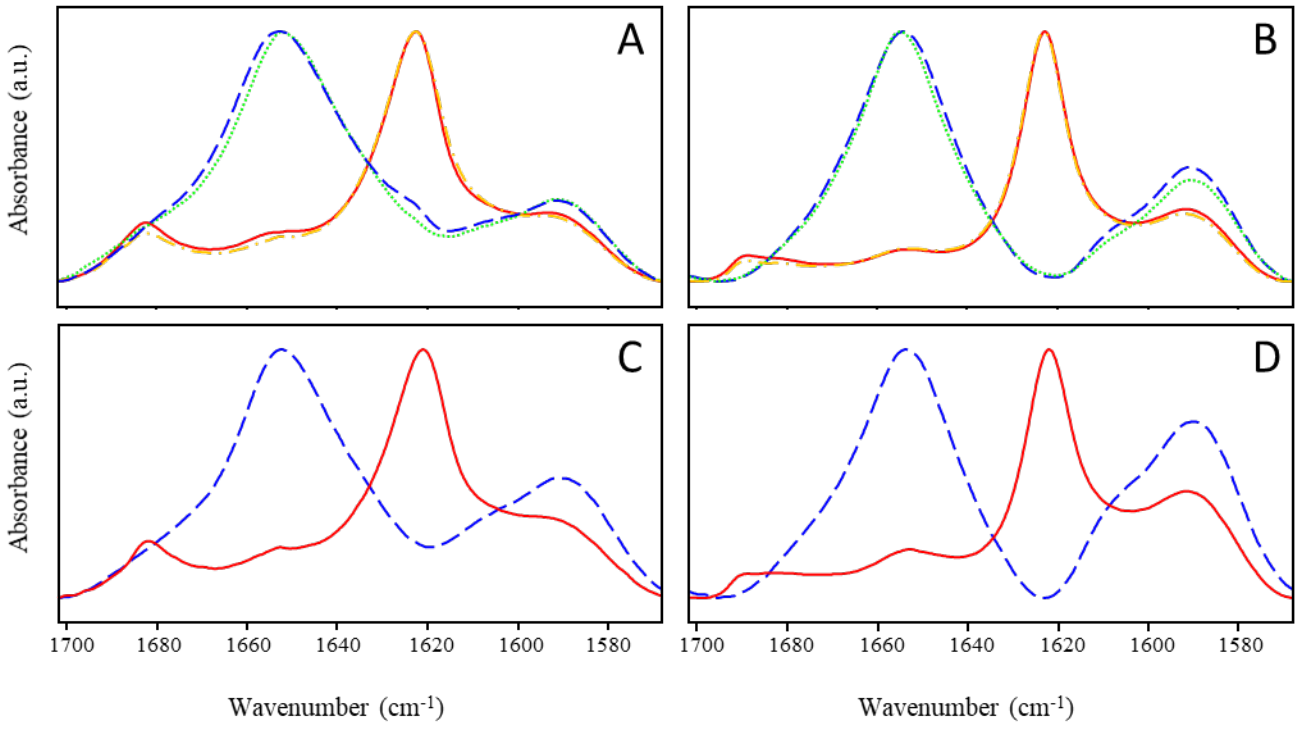

Figure 3. Infrared spectra at 37°C of the amide I' region of crown ether peptide analogues in a D_2O buffer solution at pH 7.4 in the presence of POPC (A and C) or POPG (B and D) vesicles at a P/L ratio of 1:60. Spectra A and B: R4 (—), R5 (– – –), R10 (· · ·) and R11 (– · –). Spectra C and D: R4R11 (—) and R5R10 (– – –). Spectra are normalised with respect to the amide I′ maximum.

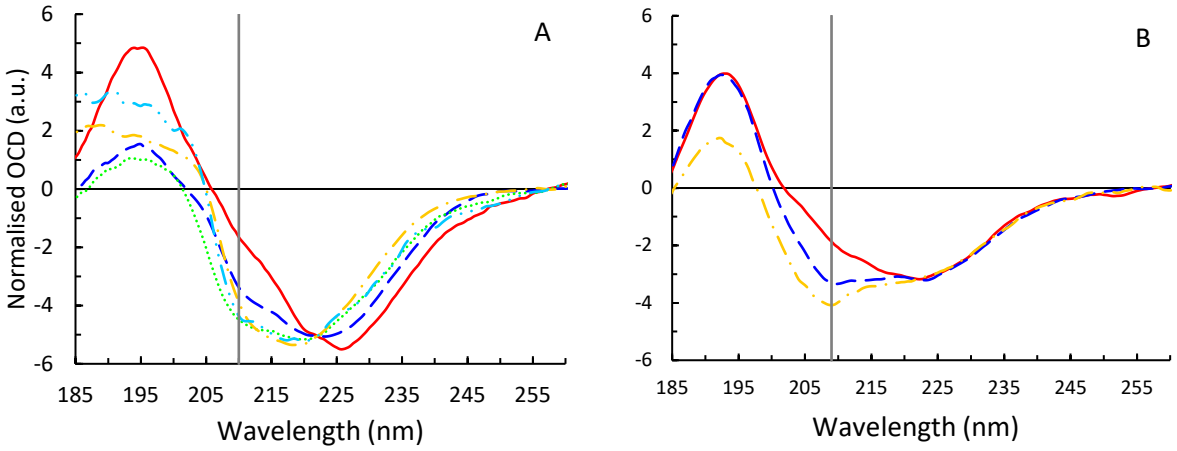

Figure 4. SR-OCD studies of peptide **1** with (A) POPC and (B) POPC/POPG 1:1 bilayers at different P:L ratios, 1:20 (—), 1:50 (– – –), 1:100 (· · ·), 1:200 (– · –), 1:500 (– · · –). The vertical line indicates the position of the minimum at 210 nm (A) or 209 nm (B); (data were normalised to have the same ellipticity at 222 nm).

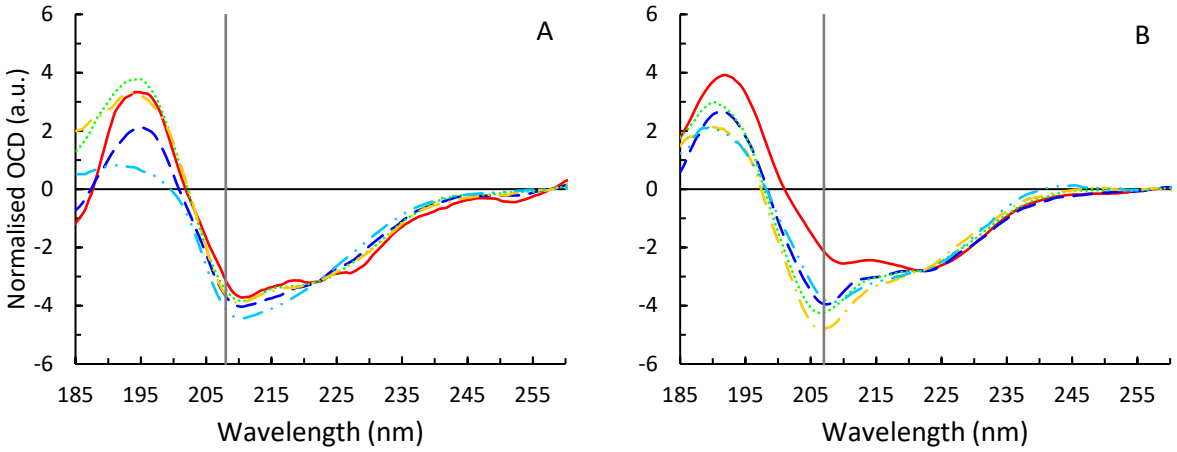

Figure 5. SR-OCD studies of peptide R5R10 with (A) POPC and (B) POPC/POPG 1:1 bilayer at different P:L ratios, 1:20 (—), 1:50 (– – –), 1:100 (· · ·), 1:200 (– · –), 1:500 (– · · –). The vertical line indicates the position of the minimum at 208 nm (A) or 207 nm (B); (data were normalised to have the same ellipticity at 222 nm).

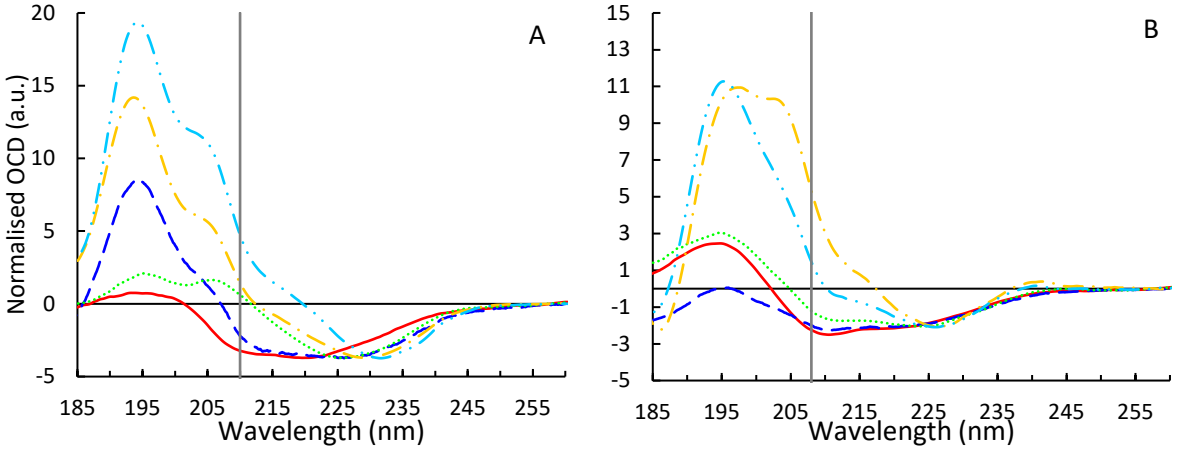

Figure 6. SR-OCD studies of peptide (A) **1** and (B) R5R10 with POPC (—), DMPC (– – –), DMoPC (· · ·), DLPC (– · –), DDPC (– · · –) bilayer at P:L ratio 1:100. The vertical line indicates the position of the minimum at 210 nm (A) and 208 nm (B); (data were normalised to have the same ellipticity at their corresponding long-wavelength minimum band).

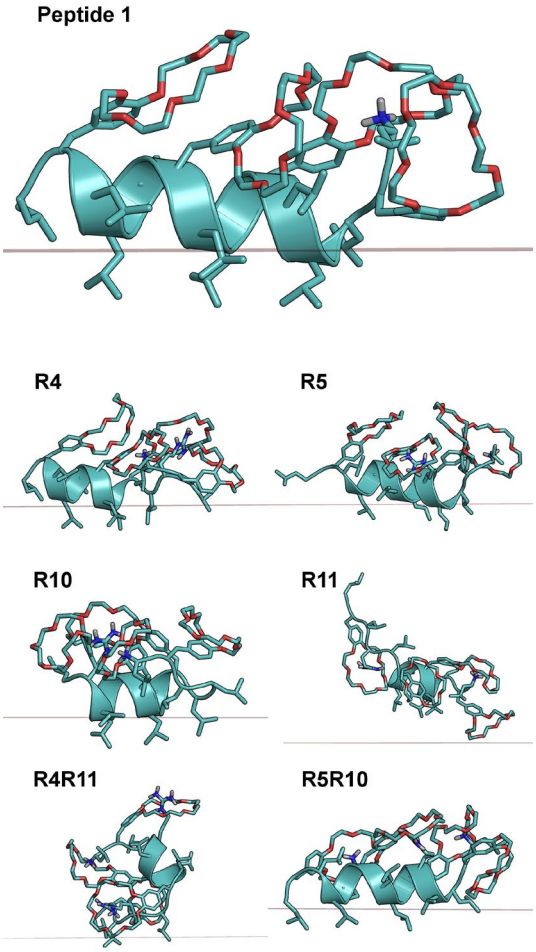

Figure 7. Typical conformation of peptide **1** and its analogues, with the standard (charged) termini, as observed from the MD trajectories. The peptides are represented as cartoon, with the side chains as sticks. Only the side chain polar hydrogens are represented for clarity. The implicit bilayer interfaces are represented by the grey lines. For the typical structures for the peptides with neutral termini, see SM Figures S9-S15.

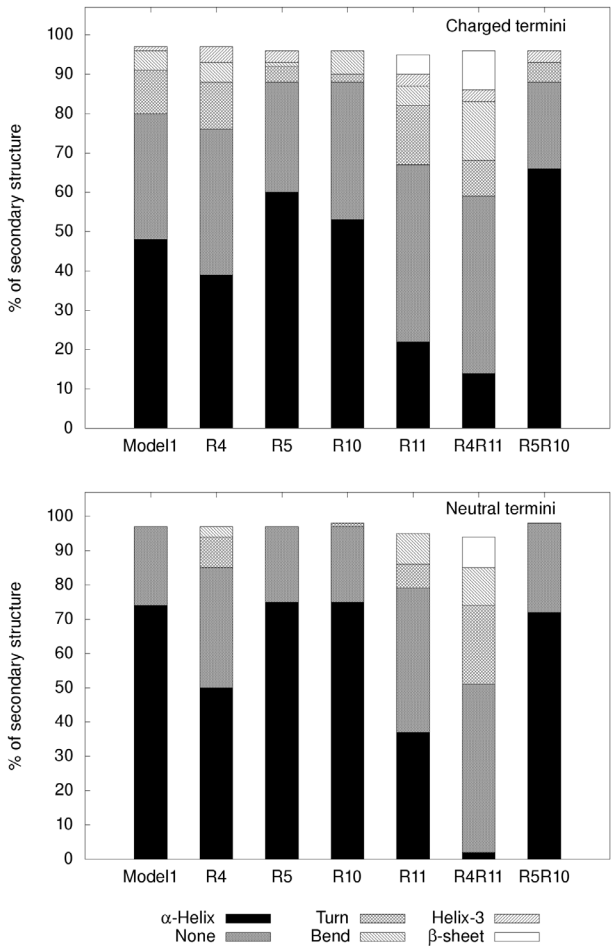

Figure 8. Secondary structure content for peptide **1** and its analogues, as calculated from the MD trajectories, for the peptides with charged (top) and neutral (bottom) termini. The percentages of secondary structures are averaged over the amino acids of each peptide. For a description of the individual secondary structure contents for each amino acid, see SM Figures S16-S22.